Modulational instability of Bose-Einstein condensates with helicoidal spin-orbit coupling

Xiao-Xun Li, Rui-Jin Cheng, Ai-Xia Zhang, and Ju-Kui Xue*
College of Physics and Electronics Engineering, Northwest Normal University, Lanzhou 730070, China

(Received 21 July 2019; published 26 September 2019)

We theoretically study the modulation instability (MI) of the two-component helicoidal spin-orbit coupled Bose-Einstein condensates (BECs). The effects of spin-orbit coupling, the helicoidal gauge potential, and atomic interactions on MI are investigated. The results indicate that the presence of the helicoidal gauge potential breaks the symmetric properties of MI, strongly modifies the distribution of the MI region and the MI gain in parameters space, and the MI can be excited even when the miscibility condition for the atomic interactions is satisfied. Furthermore, the effect of the helicoidal gauge potential on MI is strongly coupled with the intra and intercomponent atomic interactions. Particularly, with the increase of the helical gauge potential, the MI gain increases for the repulsive atomic interaction case, however, the MI gain decreases for the attractive atomic interaction case. The direct numerical simulations are performed to support the analytical predictions, and a good agreement is found. Our results provide a potential way to manipulate the MI in BECs with helicoidal gauge potential.

DOI: 10.1103/PhysRevE.100.032220

I. INTRODUCTION

Modulation instability (MI) is one of the most generic phenomenon in the propagation dynamics of any nonlinear media [1]. The MI is a result of the interplay between nonlinearity and diffraction effects, and any deviation from the steady state in the form of any weak perturbation leads to an exponential growth. The MI has been investigated in various fields such as fluid dynamics [2], magnetism [3], plasma physics [4], and Bose-Einstein condensates (BECs) [5–8]. In the context of BECs, MI has attracted great attention for a long time, owing to its fundamental and significance in various aspects. In the case of single-component BEC, MI has been addressed in many earlier works, it was concluded that the MI is possible only for BEC with attractive atomic interaction [9,10]. In the two-component BECs, the MI was first considered by Goldstein and Meystre [11], and it occurs even for condensates with repulsive interaction [12,13].

The spin-orbit (SO) coupled BECs are also one of the hottest topics of current research in the context of macroscopic quantum phenomena, and great theoretical and experimental progress have been made in this field. SO coupling describes the interaction between the particles spin and orbital momentum, it accounts for a number of fundamental phenomena in semiconductor physics, such as the spin-hall effect [14], topological superconductivity [15,16], and realization of spintronics [17]. In the two-component BECs, the experiment shows that the synthetic SO coupling can be realized by using the two Raman laser beams which couple two hyperfine ground states of the atom [18]. Due to the production of the SO coupling in BECs, the dynamical instability of supercurrents, as a consequence of the violation of the Galilean invariance, was investigated [19,20]. Meanwhile the MI of two-component BECs with SO coupling in one and two dimensions were recently investigated [21,22].

Recently, a technique showed that a proper combination of laser beams illumination can create the potentials of practically arbitrary form in atomic systems, which is possible to engineer SO coupling in BECs [18,23]. The cold atomic systems with tunable SO coupling [24–27] provide an ideal platform for investigating a wide range of interesting physics in SO-coupled systems. Based on the tunability of the SO coupling in atomic systems and the intrinsic nonlinearity of SO-coupled BECs stemming from interatomic interactions, the soliton dynamics in BECs with inhomogeneous SO coupling have been extensively studied [28,29]. In particular, the propagation of solitons in the BECs with inhomogeneous helicoidal SO coupling is addressed [29], the helicoidal gauge potential can arise in description of light propagation in helical waveguide arrays [30]. Considering the MI is a key mechanism for the formation of soliton trains in diverse physical media [31,32], and inspired by the special features of SO coupling and the physical relevance of two-component BECs system, we study the dynamical behavior of MI in helicoidal SO-coupled BECs.

In this paper, we study the MI of the two-component helicoidal SO-coupled BECs equally distributed between the two pseudospin states. A linearized Gross-Pitaevskii (GP) equation and the dispersion relation corresponding to the instability of the flat continuous wave (cw) background are obtained by considering a small perturbation approximation. We presented detailed analyses of the effects of the helicoidal gauge potential, SO coupling, and nonlinear interactions on MI in two-component BECs. We find that the helicoidal gauge potential plays an important role on the MI of the system. The helicoidal gauge potential breaks the symmetric properties of MI and the effect of the helicoidal gauge potential on MI is strongly coupled with SO coupling and the intra and intercomponent atomic interactions. The paper is structured as follows. In Sec. II, we describe the theoretical model of

*Corresponding author: xuejk@nwnu.edu.cn

the two-component BECs with helicoidal SO coupling. In this section, we also derive the dispersion relation for the MI by means of the linear-stability analysis. In Sec. III, the effects of atomic interactions, SO coupling, and helicoidal gauge potential on MI are systematically discussed and revealed. In Sec. IV, the numerical simulations of the system are presented, which confirm our theoretical prediction. The paper is concluded in Sec. V.

II. MODEL AND LINEAR-STABILITY APPROACH

We consider a one-dimensional spatially inhomogeneous two-component BECs with helicoidal SO coupling. The single-particle Hamiltonian H_0 of the system can be written as [29]

$$H_0 = \frac{[p+\alpha A(x)]^2}{2} + \frac{\Delta\sigma_z}{2}, \tag{1}$$

where $p = -i\partial/\partial x$ is the momentum operator, $A(x)$ is the spatially varying gauge potential, α is the potential amplitude, Δ is the Zeeman splitting, $\sigma_{x,y,z}$ are Pauli matrices. If the interactions among the atoms in the BECs are taken into account, in the Hartree approximation, the dimensionless GP equation describing a spinor order parameter $\mathbf{\Psi} = (\Psi_1, \Psi_2)^T$ (T stands for the transpose) can be obtained as follows:

$$i\frac{\partial \mathbf{\Psi}}{\partial t} = \frac{1}{2}\left[\frac{1}{i}\frac{\partial}{\partial x} + \alpha A(x)\right]^2 \mathbf{\Psi} + \frac{\Delta}{2}\sigma_z \mathbf{\Psi} + G\mathbf{\Psi}, \tag{2}$$

where the spatial variable x, time t, density $|\mathbf{\Psi}|^2$, and energy are expressed in normalized units $a_\perp = \sqrt{\hbar/(m\omega_\perp)}$, $\omega_\perp^{-1}(\omega_\perp$ is the transverse trap frequency), $a_\perp^{-1}$, and $\hbar\omega_\perp$, respectively, and m is the atomic mass. Here $G = \mathrm{diag}(g_1|\psi_1|^2 + g_{12}|\psi_2|^2, g_2|\psi_2|^2 + g_{12}|\psi_1|^2)$ characterizes the interatomic interaction with the interaction constants $g_{1,2} \equiv 2a_{1,2}/a_\perp$ and $g_{12} \equiv 2a_{12}/a_\perp$. The $a_{1,2}$ and a_{12} are s-wave scattering lengths, which are possible to control by optical and magnetic Feshbach resonance techniques in actual experiments [33,34].

The SO coupling, whose strength is experimentally tunable using different techniques, is considered of the helicoidal shape with the period π/β, i.e., $A(x) = \boldsymbol{\sigma}\cdot\mathbf{n}(x)$, where $\mathbf{n}(x) = [\cos(2\beta x), \sin(2\beta x), 0]$ and $\boldsymbol{\sigma} = (\sigma_x, \sigma_y, \sigma_z)$. β is the frequency of rotation, the positive and negative values of β are defined for the right-handed mode and left-handed mode, respectively [30,35,36]. The helicoidal structure of the vector potential is point translational symmetry (the shift by the period π/β). For convenience, we use gauge transformation to switch to the rotating frame for the chosen gauge field $A(x)$ [29]

$$\mathbf{\Psi} = e^{-i(\alpha^2+\beta^2)t/2} e^{-i\sigma_z\beta x}\boldsymbol{\psi}, \tag{3}$$

then the point translation symmetry of Eq. (2) becomes a continuous translational symmetry of the transformed equations, and the continuous GP equations for $\boldsymbol{\psi}$ are

$$\begin{aligned} i\frac{\partial\psi_1}{\partial t} &= -\frac{1}{2}\frac{\partial^2\psi_1}{\partial x^2} + i\beta\frac{\partial\psi_1}{\partial x} - i\alpha\frac{\partial\psi_2}{\partial x} + \frac{\Delta}{2}\psi_1 \\ &\quad + (g_1|\psi_1|^2 + g_{12}|\psi_2|^2)\psi_1, \end{aligned} \tag{4}$$

$$\begin{aligned} i\frac{\partial\psi_2}{\partial t} &= -\frac{1}{2}\frac{\partial^2\psi_2}{\partial x^2} - i\beta\frac{\partial\psi_2}{\partial x} - i\alpha\frac{\partial\psi_1}{\partial x} - \frac{\Delta}{2}\psi_2 \\ &\quad + (g_2|\psi_2|^2 + g_{12}|\psi_1|^2)\psi_2, \end{aligned} \tag{5}$$

where α represents the SO coupling, β represents the helicoidal gauge potential. The total number of atoms are

$$N = \int dx(|\psi_1|^2 + |\psi_2|^2) = N_1 + N_2. \tag{6}$$

In the framework of Eqs. (4) and (5), the MI of the cw state in the form of a miscible binary condensate with uniform densities n_{10}, n_{20} and the common chemical potential μ of both components: $\psi_j = e^{-i\mu t}\sqrt{n_{j0}}$. The densities, Zeeman splitting, interactions, and chemical potential are determined by algebraic equations:

$$\frac{\Delta}{2} = (-1)^j(g_j n_{j0} + g_{12}n_{3-j,0} - \mu), \qquad j = 1, 2. \tag{7}$$

For the investigation of MI in the helicoidal SO-coupled BECs, we add the small perturbations $\delta\psi_j$ ($\delta\psi_j \ll \sqrt{n_{j0}}$) to the cw solutions: $\psi_j = e^{-i\mu t}(\sqrt{n_{j0}} + \delta\psi_j)$. Linearized equations for the small perturbations are as follows:

$$\begin{aligned} i\frac{\partial(\delta\psi_1)}{\partial t} &= -\frac{1}{2}\frac{\partial^2(\delta\psi_1)}{\partial x^2} - i\alpha\frac{\partial(\delta\psi_2)}{\partial x} + i\beta\frac{\partial(\delta\psi_1)}{\partial x} \\ &\quad + g_1 n_{10}(\delta\psi_1^* + \delta\psi_1) + g_{12}\sqrt{n_{10}n_{20}}(\delta\psi_2^* + \delta\psi_2), \end{aligned} \tag{8}$$

$$\begin{aligned} i\frac{\partial(\delta\psi_2)}{\partial t} &= -\frac{1}{2}\frac{\partial^2(\delta\psi_2)}{\partial x^2} - i\alpha\frac{\partial(\delta\psi_1)}{\partial x} - i\beta\frac{\partial(\delta\psi_2)}{\partial x} \\ &\quad + g_2 n_{20}(\delta\psi_2^* + \delta\psi_2) + g_{12}\sqrt{n_{10}n_{20}}(\delta\psi_1^* + \delta\psi_1), \end{aligned} \tag{9}$$

where $\boldsymbol{\psi}^*$ stands for the complex conjugate of $\boldsymbol{\psi}$. We assume the solution of the perturbation in the form of plane waves

$$\delta\psi_j = \zeta_j\cos(kx - \Omega t) + i\eta_j\sin(kx - \Omega t), \tag{10}$$

where k is real wave number, Ω is complex eigenfrequency, ζ_j and η_j are amplitudes. A set of linearly coupled equations for perturbation amplitudes ζ_j and η_j are derived by substituting Eq. (10) in Eqs. (8) and (9):

$$\mathbf{M}\times(\zeta_1, \zeta_2, \eta_1, \eta_2)^T = 0, \tag{11}$$

where $\mathbf{M}$ is a 4×4 matrix, it exists in a nontrivial solution under condition with $\det\mathbf{M} = 0$ and we can obtain the dispersion relation of the system for Ω:

$$\Omega^4 + P_2\Omega^2 + P_1\Omega + P_0 = 0, \tag{12}$$

where $P_2 = -2k^2(\alpha^2+\beta^2) - k^2(g_1n_{10} + g_2n_{20}) - k^4/2$, $P_1 = 2k^3[\beta(g_1n_{10} - g_2n_{20}) - 2\alpha g_{12}\sqrt{n_{10}n_{20}}]$, $P_0 = k^4/16\{[k^2 - 4(\alpha^2+\beta^2) + 4g_1n_{10}][k^2 - 4(\alpha^2+\beta^2) + 4g_2n_{20}] - 16g_{12}^2n_{10}n_{20}\}$. Solving Eq. (12), we can obtain the analytical results

$$\Omega_{1,2} = \frac{1}{2}\sqrt{\frac{-2P_2}{3} + \Lambda} \mp \frac{1}{2}\sqrt{\frac{-4P_2}{3} - \Lambda + \frac{2P_1}{\sqrt{\frac{-2P_2}{3} + \Lambda}}}, \tag{13}$$

$$\Omega_{3,4} = \frac{-1}{2}\sqrt{\frac{-2P_2}{3} + \Lambda} \mp \frac{1}{2}\sqrt{\frac{-4P_2}{3} - \Lambda - \frac{2P_1}{\sqrt{\frac{-2P_2}{3} + \Lambda}}}, \tag{14}$$

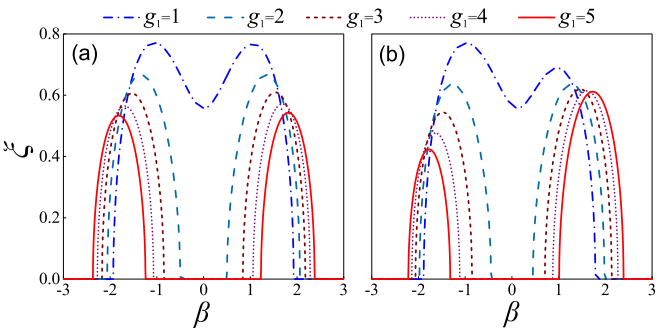

FIG. 1. The MI gain ξ as a function of helicoidal gauge potential β for different intracomponent interaction g_1, with (a) $\alpha = 0.025$ and (b) $\alpha = 0.5$. Here, $k = 1$, $g_2 = 2$, and $g_{12} = 2$.

here the coefficients Λ, Λ_1, and Λ_2 are given by

$$\Lambda = \frac{\sqrt[3]{2}\Lambda_1}{3\sqrt[3]{\Lambda_2 + \sqrt{-4\Lambda_1^3 + \Lambda_2^2}}} + \frac{\sqrt[3]{\Lambda_2 + \sqrt{-4\Lambda_1^3 + \Lambda_2^2}}}{3\sqrt[3]{2}}, \quad (15)$$

$$\Lambda_1 = P_2^2 + 12P_0, \; \Lambda_2 = 2P_2^3 + 27P_1^2 - 72P_0P_2. \quad (16)$$

From Eqs. (13) and (14), the value of the Ω may be positive, negative, or complex, depending on the signs and magnitudes of the terms involved. The cw state is stable when Ω is real, otherwise, MI takes place. The instability growth rate of MI is defined as

$$\xi = \{|\mathrm{Im}(\Omega)|\}_{\max}. \quad (17)$$

Equations (13) and (14) reveal that different physical effects inevitably affect the instability of the system. The dispersion relation and the instability spectra are substantially influenced by SO coupling and helicoidal gauge potential. Noting that the parameter Δ has not appeared in the dispersion relation for instability and it means that it cannot affect the properties of the MI for cw in such system. Meanwhile, the nature of the atomic interactions' strength is found to be fundamental to the existence of MI and it plays a crucial role in characterizing the instability spectra. The commonly known case of the MI in the two-component model, which corresponds to $\alpha = \beta = 0$, is reproduced by the above results: it occurs for $g_{12}^2 > g_1 g_2$ (interactions are repulsive) in the interval of perturbation wave numbers $0 < k < [2(\sqrt{(g_1 n_{10} - g_2 n_{20})^2 + 4g_{12}^2 n_{10} n_{20}} - g_1 n_{10} - g_2 n_{20})]^{1/2}$ [12]. For convenience, we assume the density of the two components equal to 1, that is, $n_{10} = n_{20} = 1$. In this paper, we would like to discuss the influence of different physical effects on the instability spectrum.

III. ANALYSIS OF THE MI

A. Effect of the atomic interactions on the MI

In this section, the influence of the atomic interactions on the MI is investigated and analyzed. At first, we discuss the MI of the system when both the intra and intercomponent interactions are repulsive. Figure 1 shows the MI gain as a function of the helicoidal gauge potential β for different values of intracomponent interaction g_1 and SO coupling strength α at fixed other parameters $g_2 = 2$, $g_{12} = 2$, and $k = 1$. The MI gain ξ decreases gradually with the increase of intracomponent interaction g_1, and the instable region for β changes from a single region with multipeak to multiple regions when $g_1 g_2 \geqslant g_{12}^2$. It is well known that when the SO coupling is absent, i.e., $\alpha = \beta = 0$, the MI immiscibility condition is $g_{12}^2 > g_1 g_2$ for the binary condensates with repulsive interactions. However, Fig. 1 indicates that the system still exhibits MI under $g_1 g_2 \geqslant g_{12}^2$ due to the appearance of the SO coupling α and the helicoidal gauge potential β. The above results suggest that the MI in the miscibility condition is still possible even in the repulsive two-component BECs with helicoidal SO coupling.

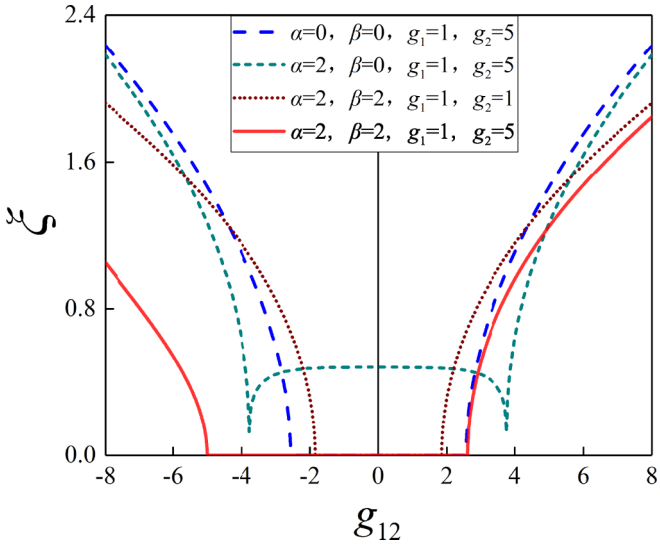

FIG. 2. The MI gain ξ against g_{12} for different physical parameters with $k = 1$.

It is interesting to note that the MI gain ξ and the MI region for β are symmetry about $\beta = 0$ when $\alpha \to 0$ [see Fig. 1(a)], or when $g_1 = g_2$ [see Fig. 1(b)]. However, as the SO coupling α increases [see Fig. 1(b)], the symmetry is broken. When $g_1 < g_2$, the MI gain for $\beta < 0$ is larger than that for $\beta > 0$. However, when $g_1 > g_2$, the MI gain and the MI region of β for $\beta < 0$ is smaller than that for $\beta > 0$, and the reduction rate of the MI gain ξ with g_1 in the range of $\beta < 0$ is larger than that in the range of $\beta > 0$. That is, the MI properties is different in the system with right-handed and left-handed helicoidal SO coupling. To interpret the symmetry of the MI regions in Fig. 1, we make the following analysis. From Eqs. (12) to (16) we can find that the symmetry of MI about β is described by the parameter P_1. Replacing the coefficient P_1 with $-P_1$ in Eqs. (12) to (16), we obtain

$$\Omega_1' = -\Omega_4, \quad \Omega_2' = -\Omega_3,$$
$$\Omega_3' = -\Omega_2, \quad \Omega_4' = -\Omega_1. \quad (18)$$

It can be obtained from the definition of modulation instability $\xi = \{|\mathrm{Im}(\Omega)|\}_{\max}$ that the MI gain ξ of the system is not affected when P_1 is set to $-P_1$. As we assumed $n_{10} = n_{20} = 1$, then we have

$$P_1(X) = 2k^3[\beta(g_1 - g_2) - 2\alpha g_{12}], \quad (19)$$

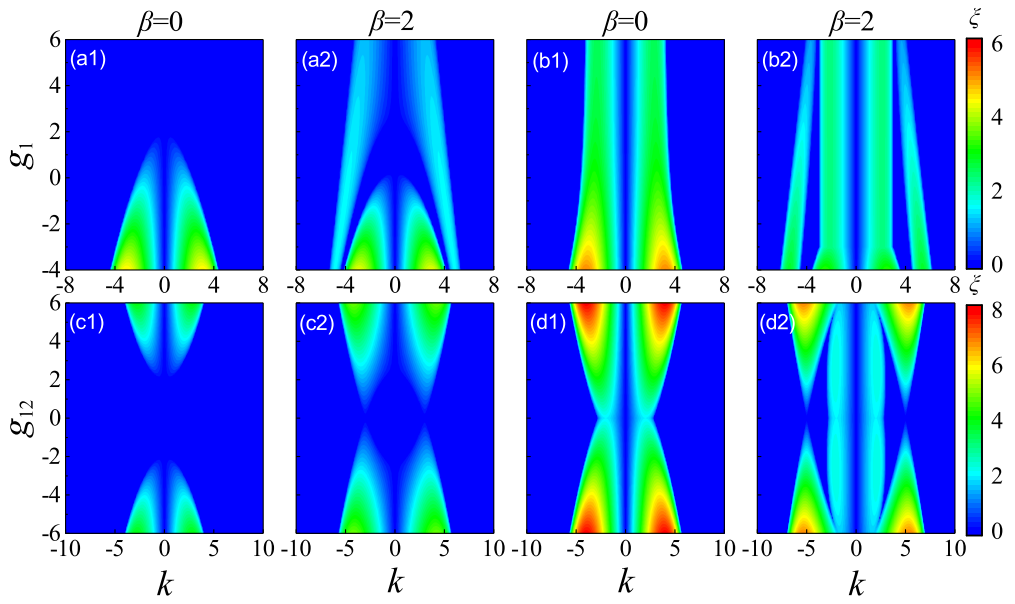

FIG. 3. The first row: The contour plot of the MI gain ξ in the (k, g_1) plane for fixed other interaction parameters, in (a1)–(a2): $g_2 = g_{12} = 2$, and in (b1)–(b2): $g_2 = g_{12} = -2$. The second row: The contour plot of the MI gain ξ in the (k, g_{12}) plane for fixed other interaction parameters, in (c1)–(c2): $g_1 = g_2 = 2$, and in (d1)–(d2): $g_1 = g_2 = -2$. In all cases $\alpha = 0.5$.

where X refers to any variable in P_1. Naturally, we can obtain that the MI gain ξ will be symmetric about X when $P_1(X)$ satisfy the following condition:

$$|P_1(-X)| = |P_1(X)|. \tag{20}$$

Clearly, as shown in Fig. 1, when $\alpha \to 0$ or $g_1 = g_2$, one has $|P_1(-\beta)| = |P_1(\beta)|$. Therefore, the region of the MI and the MI gain are symmetric about $\beta = 0$ in both cases. Equation (19) indicates that the asymmetry of MI about $\beta = 0$ is different for $g_1 > g_2$ and $g_1 < g_2$ [see also Fig. 1(b)]. Particularly, Eq. (19) indicates that, when $\beta = \alpha = 0$ or $\beta = 0$ or $g_1 = g_2$, the MI is symmetric about $g_{12} = 0$ ($|P_1(-g_{12})| = |P_1(g_{12})|$), otherwise, the presence of the helicoidal gauge potential β ($g_1 \neq g_2$) breaks this symmetry, i.e., the MI for $g_{12} < 0$ and $g_{12} > 0$ is different. This is clearly shown in Fig. 2. When $g_1 = g_2$ and $\beta \neq 0$, the MI gain and the threshold of g_{12} for the occurrence of MI are not symmetric about $g_{12} = 0$. The asymmetry of MI induced by the helicoidal gauge potential in parameter space will be further demonstrated in the following subsection.

The MI discussed above is mainly focused on the cases when the intracomponent interaction is repulsive, and now we discuss it in general interactions' cases. Figures 3(a1) to 3(a2) and Figures 3(b1) to 3(b2) show the MI gain in the (k, g_1) plane when the intra (g_2) and intercomponent (g_{12}) interactions are repulsive and attractive, respectively. Figures 3(c1) and 3(c2) and Figures 3(d1) and 3(d2) show the MI gain in the (k, g_{12}) plane when the intracomponent interactions g_1, g_2 are repulsive and attractive, respectively. In this case, we choose $g_1 = g_2$, and the MI region is symmetrical about $g_{12} = 0$ from the previous analysis. Figure 3 shows that the atomic interactions significantly affect the development of the MI, and the presence of the helicoidal gauge potential greatly enriches the region of the MI and affects its intensity. In the next section, we will discuss the effect of the SO coupling α and the helicoidal gauge potential β on the MI in detail.

B. Effect of SO coupling and helicoidal gauge potential on the MI

To explore the coupled effect of the SO coupling and the helicoidal gauge potential, Fig. 4 illustrates the MI gain ξ in the (α, β) plane with different wave numbers k when the interactions are repulsive and satisfy the condition of $g_{12}^2 \leqslant g_1 g_2$. Figure 4 shows that the MI takes place when α and β satisfy certain conditions. There exists a set of the symmetrical MI region of crescent shape in the (α, β) plane and the slope of the symmetry axis is related to the strength of the interactions. As seen in Fig. 4(a1), we arbitrarily select four points in the (α, β) plane which are symmetrical with each other, and these

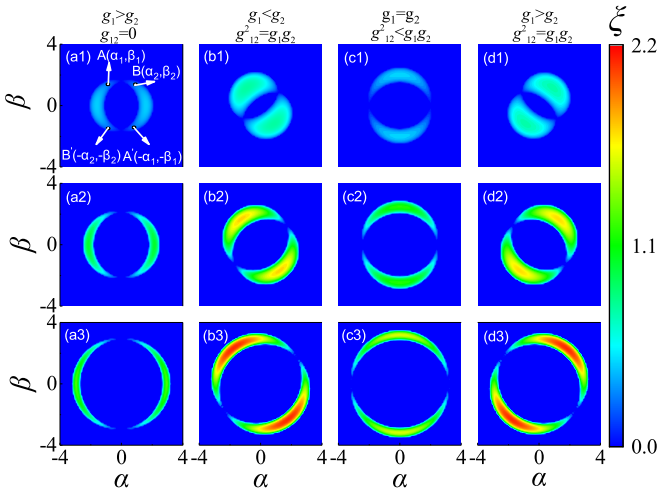

FIG. 4. The contour plot of the MI gain ξ as a function of α and β. The first column for $g_1 = 4$, $g_2 = 1$, and $g_{12} = 0$. The second column for $g_1 = 1$, $g_2 = 4$, and $g_{12} = 2$. The third column for $g_1 = 4$, $g_2 = 4$, and $g_{12} = 2$. The last column for $g_1 = 4$, $g_2 = 1$, and $g_{12} = 2$. The first (second, third) row for $k = 1$ ($k = 3$, $k = 5$).

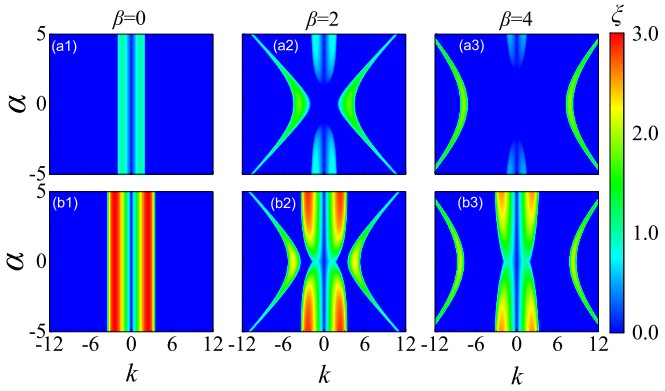

FIG. 5. The contour plot of the MI gain ξ in the (k, α) plane for fixed interactions. In (a1)–(a3): $g = 1$, $g_{12} = 2$. In (b1)–(b3): $g = -1$, $g_{12} = -2$.

points satisfy the following conditions: $\alpha_1^2 + \beta_1^2 = \alpha_2^2 + \beta_2^2$ and $P_1(\alpha_1, \beta_1) = P_1(\alpha_2, \beta_2) = -P_1(-\alpha_1, -\beta_1) = -P_1(-\alpha_2, -\beta_2)$. The symmetry axis of the MI region is perpendicular to the straight line AB and $B'A'$, therefore, the slope R of the symmetry axis is

$$R = \frac{d\beta}{d\alpha} = \frac{g_2 - g_1}{2g_{12}}. \tag{21}$$

The slope R is irrelevant of the wave number k, and we will discuss it in the following four cases.

(i)When the intercomponent interaction is not considered ($g_{12} = 0$), $P_1(\alpha)$ and $P_1(\beta)$ satisfy the symmetric condition Eq. (20), i.e., $P_1(-\alpha) = P_1(\alpha)$, and $P_1(-\beta) = P_1(\beta)$. So the MI region is symmetric with respect to $\alpha = 0$ ($R \to \infty$) and $\beta = 0$, as shown in Figs. 4(a1) to 4(a3). It can also be seen that the system is always stable at $\alpha \to 0$ regardless of the value of β. Under the condition of $g_{12} = 0$, $\alpha \to 0$, Eqs. (13) and (14) can be simplified to

$$\Omega_{1,2} = -k\beta \mp \frac{k}{2}\sqrt{k^2 + 4g_1},$$
$$\Omega_{3,4} = k\beta \mp \frac{k}{2}\sqrt{k^2 + 4g_2}, \tag{22}$$

here $g_1 > 0$, $g_2 > 0$. Equation (22) indicates that $\Omega_{1,2}$ and $\Omega_{3,4}$ are always real, i.e., $\xi = 0$. The system is stable.

When the intercomponent interaction $g_{12} > 0$, the symmetrical region of MI in the (α, β) plane can be divided into the following three cases according to the intensity of the atomic intracomponent interactions.

(ii) When $g_1 < g_2$, it can be obtained from Eq. (21) that the slope R of the symmetric axis of the MI region is positive, as shown in Figs. 4(b1) to 4(b3). When $\alpha \neq 0$, the MI is asymmetric about $\beta = 0$. The intensity of the MI is greater when the sign of α and β is opposite.

(iii) When $g_1 = g_2 = g$, as mentioned in the previous section, the MI region in the (α, β) plane is symmetric with respect to $\beta = 0$ ($R = 0$) and $\alpha = 0$, as shown in Figs. 4(c1) to 4(c3). Particularly, the system is always stable at $\beta = 0$ regardless of the value of the SO coupling strength α. Under the condition of $g_1 = g_2 = g$, $\beta = 0$, Eqs. (13) and (14) can

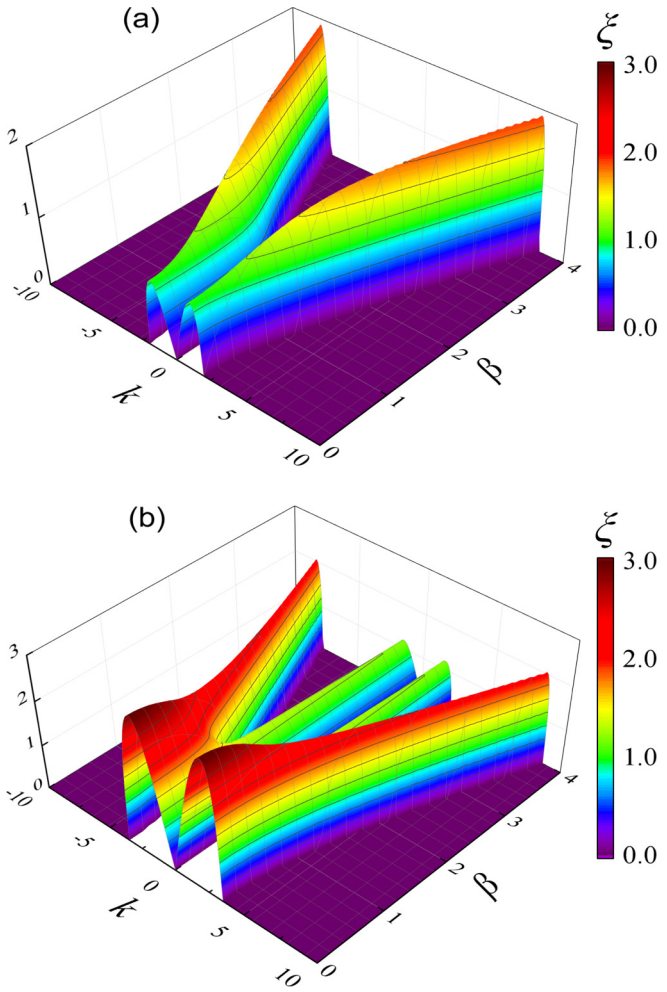

FIG. 6. The change of the MI gain ξ with the variation of β for fixed interactions. In (a): $g_1 = g_2 = g = 1$ and $g_{12} = 2$. In (b): $g_1 = g_2 = g = -1$ and $g_{12} = -2$. In all cases $\alpha = 0.5$.

be simplified to

$$\Omega_{1,2} = -k\alpha \mp \frac{k}{2}\sqrt{k^2 + 4(g - g_{12})},$$
$$\Omega_{3,4} = k\alpha \mp \frac{k}{2}\sqrt{k^2 + 4(g + g_{12})}, \tag{23}$$

when $g \geqslant g_{12} > 0$, Eq. (23) shows that $\Omega_{1,2}$ and $\Omega_{3,4}$ are always real, i.e., $\xi = 0$. The system is stable.

(iv) When $g_1 > g_2$, it can be obtained from Eq. (21) that the slope R of the symmetric axis of the MI region is negative, as shown in Figs. 4(d1) to 4(d3). When $\alpha \neq 0$, the MI is asymmetric about $\beta = 0$. In this case, the intensity of the MI is greater when the sign of α and β is identical.

Figure 4 also indicates that the MI gain ξ increases gradually and the distribution region of MI gradually diffuses outward in the (α, β) plane with the increase of wave number k for all cases. More importantly, Fig. 4 shows that the system remains stable when both α and β are zero. It can be explained that the appearance of the SO coupling and the helicoidal gauge potential change the well-known condition in which the MI occurs in $g_{12}^2 > g_1 g_2$ when the interactions are all repulsive.

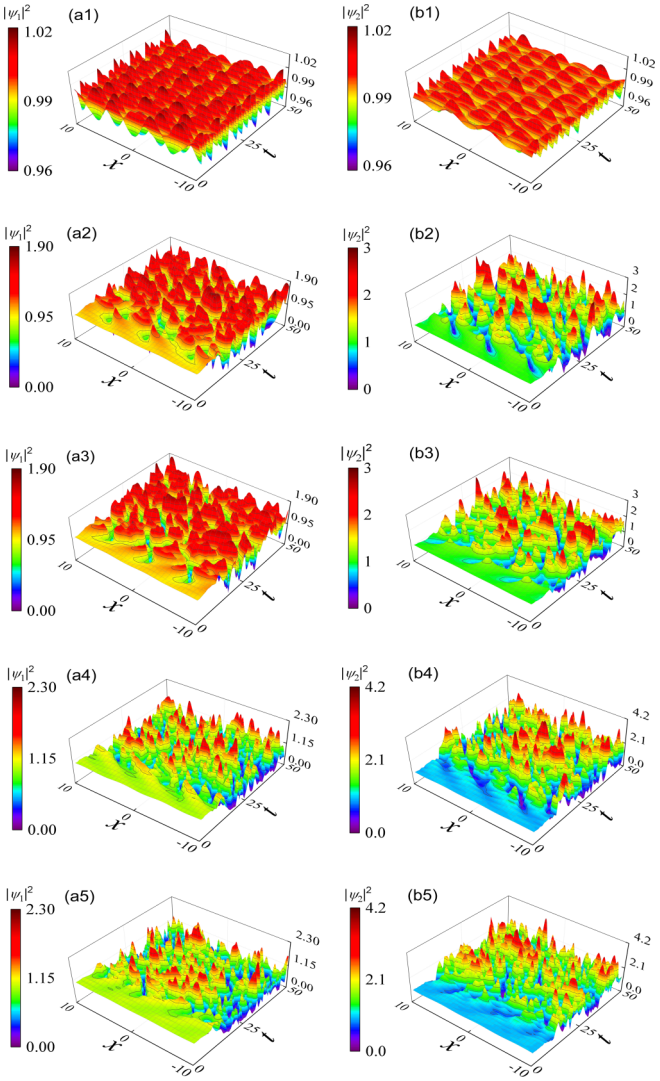

FIG. 7. The space-time evolution of cw in the different SO coupling α and helicoidal gauge potential β. (a1)–(b1): $\alpha = 0$ and $\beta = 0$. (a2)–(b2): $\alpha = 0$ and $\beta = 1.5$. (a3)–(b3): $\alpha = 0$ and $\beta = -1.5$. (a4)–(b4): $\alpha = 0.5$ and $\beta = 1.5$. (a5)–(b5): $\alpha = 0.5$ and $\beta = -1.5$. In all cases $g_1 = 5$, $g_2 = 2$, $g_{12} = 2$, and $k = 1$.

We also plot the MI gain ξ in the plane of (k, α) with different β values. For convenience, we assume the intracomponent interactions $g_1 = g_2 = g$ in the following study. The first row of Fig. 5 and the second row of that indicate the change of the MI gain ξ with β when the interactions are repulsive and attractive, respectively. As shown in Figs. 5(a1) and 5(b1), the MI gain ξ and the MI region in the (k, α) plane remain constant with the increase of α when $\beta = 0$. In this case, it can be obtained from Eq. (23) that the MI gain $\xi = \{|\mathrm{Im}(\Omega)|\}_{\max}$ is independent of α. In the presence of the helicoidal gauge potential β, Figs. 5(a2) and 5(a3) and Figs. 5(b2) and 5(b3) show that the situation is changed significantly. The MI region in the (k, α) plane is modified by the helicoidal gauge potential and strongly depends on α and β, especially for the repulsive interactions case (the first row of Fig. 5). It can also see that the intensity of MI in the attractive interactions is greater than that in the repulsive interactions case.

To emphasize the effect of β on the MI, we plot the change of the MI gain ξ with the variation of $\beta > 0$ for fixed interactions due to the MI region mentioned above is symmetric about $\beta = 0$. Figure 6 illustrates the MI gain ξ in the (k, β) plane when the atomic interactions are repulsive [Fig. 6(a)] and attractive [Fig. 6(b)], respectively. As shown in Fig. 6(a), as the strength of β increases, the MI gain ξ of the system increases gradually and the MI region for k shrinks and shifts toward large $|k|$ region. However, Fig. 6(b) shows the MI gain ξ of the system decreases with the increase of β. The MI regions change from two to four and the outer band diffuses outward. Overall, Fig. 6 shows that the MI gain ξ increases with β when the interactions are repulsive. However, it decreases with β when the interactions are attractive. This conclusion can also be well confirmed by Fig. 5.

IV. NUMERICAL RESULTS

The dynamically instability predicted by the linear stability analysis can be confirmed by the time and space evolution of the cw via the directly numerical simulation of Eqs. (4) and (5). Initially we set $\psi_1(x, 0) = \psi_2(x, 0) = \psi_0 + \varepsilon \cos(kx)$, where the wave amplitude $\psi_0 = 1$ and the perturbation amplitude $\varepsilon = 0.01$, which is sufficiently small and will not cause significant variation in the qualitative nature of the results. The value of Δ is 0.01 in all numerical simulations.

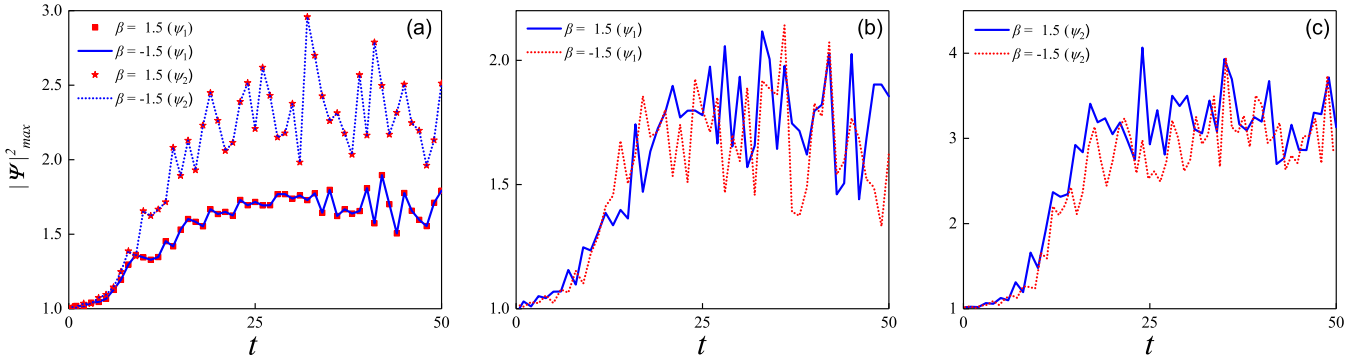

FIG. 8. The time evolution of the maximum modulus square $|\boldsymbol{\psi}|^2$ with SO coupling α and helicoidal gauge potential β as used in Figs. 7(a2) to 7(a5) and Figs. 7(b2) to 7(b5). (a): $\alpha = 0$. (b)–(c): $\alpha = 0.5$. In all cases $g_1 = 5$, $g_2 = 2$, $g_{12} = 2$, and $k = 1$.

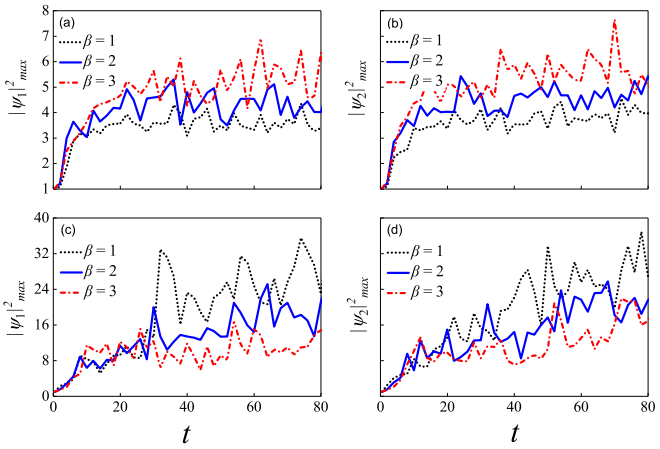

FIG. 9. The time evolution of the maximum modulus square $|\boldsymbol{\psi}|^2$ with different helicoidal gauge potential β. (a, b): $g_1 = g_2 = g = 1$ and $g_{12} = 2$. (c, d): $g_1 = g_2 = g = -1$ and $g_{12} = -2$. In all cases $\alpha = 0.5$.

For instance, Fig. 7 demonstrates the evolution of the square amplitude of the cw in the system in time and space for different SO coupling α and helicoidal gauge potential β. When the two-component BECs satisfy the miscibility condition ($g_1 g_2 > g_{12}^2$), we generally expect the condensates to be stable. As can be seen from Figs. 7(a1) and 7(b1), with the miscibility condition (i.e., $g_1 = 5$, $g_2 = 2$, $g_{12} = 2$, see Fig. 1), and in the absence of helicoidal gauge potential and the strength of SO coupling is extremely weak (i.e., $\beta = 0$, $\alpha \to 0$), the density in both condensates performs only a small oscillation that does not bring the system away from its initial state, thus, the system is stable. However, the stability is strongly affected when the helicoidal gauge potential comes into play, and the density perturbation grows exponentially, this means that the MI is excited [see Figs. 7(a2) and 7(b2) and Figs. 7(a3) and 7(b3)]. Furthermore, one can find that, when the SO coupling $\alpha \to 0$, the MI for the system has a similar character for the right-handed ($\beta > 0$) and left-handed ($\beta < 0$) of the helicoidal gauge potential. To observe the phenomenon more clearly, we illustrate the time evolution of the maximum modulus square $|\boldsymbol{\psi}|^2$ of Figs. 7(a2) and 7(a3) and Figs. 7(b2) and 7(b3) in Fig. 8(a) and observe that the $|\boldsymbol{\psi}|^2_{\max}$ for the right-handed and left-handed helicoidal gauge potential is coincident. However, Figs. 7(a4) and 7(a5) and Figs. 7(b4) and 7(b5) show that the right-handed and left-landed helicoidal gauge potential have different effects on the MI for the system with larger SO coupling strength, and the time evolution of the maximum modulus square $|\boldsymbol{\psi}|^2$ of them are also shown in Figs. 8(b) and 8(c), respectively. It can be clearly found that the $|\boldsymbol{\psi}|^2_{\max}$ for different signs of the helicoidal gauge potential β is inconsistent, and the $|\boldsymbol{\psi}|^2_{\max}$ for the right-handed helicoidal gauge potential is larger than that for the left-hand one. All these results are in good agreement with the theoretical analysis shown in Fig. 1.

Figure 9 shows the time evolution of the maximum modulus square $|\boldsymbol{\psi}|^2$ for different helicoidal gauge potential β with the parameter values of Fig. 6. It can be seen from Fig. 9 that the $|\boldsymbol{\psi}|^2$ of the cw increases gradually as the strength of helicoidal gauge potential β increases when the atomic interactions are repulsive [see Figs. 9(a) and 9(b)], and decreases gradually with β when the atomic interactions are attractive [see Figs. 9(c) and 9(d)]. The numerical results are also consistent with those in Fig. 6.

V. CONCLUSION

In summary, we study the modulation instability of the spatially inhomogeneous two-component BECs with the helicoidal SO coupling by linear-stability approach. The dispersion relation corresponding to the instability of the flat continuous wave background against small perturbation is obtained. For comprehensive research, we analyze the effects of the helicoidal gauge potential, the SO coupling, and different atomic interactions on the MI. Our analysis illustrates that the presence of the helicoidal gauge potential inevitably affects the distribution of the MI region and the MI immiscibility condition is no longer significant for the system with repulsive interactions. In particular, the MI gain increases as the helicoidal gauge potential increases when the atomic interactions are repulsive. However, it decreases as the helicoidal gauge potential increases when the atomic interactions are attractive. The numerical calculations are consistent with the theoretical researches. The present results could potentially provide ways to generate and manipulate MI and solitons in the helicoidal SO coupling BECs.

ACKNOWLEDGMENTS

This work is supported by the National Natural Science Foundation of China under Grants No. 11764039, No. 11847304, No. 11865014, No. 11475027, No. 11305132, and No. 11274255, by Natural Science Foundation of Gansu province under Grant No. 17JR5RA076, and by Scientific research project of Gansu higher education under Grant No. 2016A-005.

[1] V. E. Zakharov and L. A. Ostrovsky, Physica D (Amsterdam) **238**, 540 (2009).
[2] M. Brunetti and J. Kasparian, Phys. Lett. A **378**, 3626 (2014).
[3] Z. A. Assalauov and V. E. Zakharov, Sov. J. Plasma Phys. **11**, 762 (1985).
[4] T. Taniuti and H. Washimi, Phys. Rev. Lett. **21**, 209 (1968).
[5] I. Kourakis, P. K. Shukla, M. Marklund, and L. Stenflo, Eur. Phys. J. B **46**, 381 (2005)
[6] V. V. Konotop and M. Salerno, Phys. Rev. A **65**, 021602(R) (2002).
[7] L. Li, Z. Li, B. A. Malomed, D. Mihalache, and W. M. Liu, Phys. Rev. A **72**, 033611 (2005).
[8] E. Wamba, A. Mohamadou, and T. C. Kofané, J. Phys. B **41**, 225403 (2008).
[9] G. Theocharis, Z. Rapti, P. G. Kevrekidis, D. J. Frantzeskakis, and V. V. Konotop, Phys. Rev. A **67**, 063610 (2003).

[10] L. Salasnich, A. Parola, and L. Reatto, Phys. Rev. Lett. **91**, 080405 (2003).
[11] E. V. Goldstein and P. Meystre, Phys. Rev. A **55**, 2935 (1997).
[12] K. Kasamatsu and M. Tsubota, Phys. Rev. Lett. **93**, 100402 (2004).
[13] K. Kasamatsu and M. Tsubota, Phys. Rev. A **74**, 013617 (2006).
[14] Y. K. Kato, R. C. Myers, A. C. Gossard, and D. D. Awschalom, Science **306**, 1910 (2004).
[15] M. Z. Hasan and C. L. Kane, Rev. Mod. Phys. **82**, 3045 (2010).
[16] C.-F. Liu, G. Juzeliunas, and W. M. Liu, Phys. Rev. A **95**, 023624 (2017); W. Han, G. Juzeliunas, W. Zhang, and W. M. Liu, *ibid.* **91**, 013607 (2015).
[17] C. H. L. Quay, T. L. Hughes, J. A. Sulpizio, L. N. Pfeiffer, K. W. Baldwin, K. W. West, D. Goldhaber-Gordon, and R. de Picciotto, Nat. Phys. **6**, 336 (2010).
[18] Y. J. Lin, K. Jiménez-García, and I. B. Spielman, Nature (London) **471**, 83 (2011).
[19] T. Ozawa, L. P. Pitaevskii, and S. Stringari, Phys. Rev. A **87**, 063610 (2013).
[20] S. Gautam and S. K. Adhikari, Phys. Rev. A **90**, 043619 (2014).
[21] I. A. Bhat, T. Mithun, B. A. Malomed, and K. Porsezian, Phys. Rev. A **92**, 063606 (2015).
[22] S. Bhuvaneswari, K. Nithyanandan, P. Muruganandam, and K. Porsezian, J. Phys. B **49**, 245301 (2016).
[23] J. Ruseckas, G. Juzeliūnas, P. Öhberg, and M. Fleischhauer, Phys. Rev. Lett. **95**, 010404 (2005).
[24] J. Struck, C. Ölschläger, M. Weinberg, P. Hauke, J. Simonet, A. Eckardt, M. Lewenstein, K. Sengstock, and P. Windpassinger, Phys. Rev. Lett. **108**, 225304 (2012).
[25] Y. Zhang, G. Chen, and C. Zhang, Sci. Rep. **3**, 1937 (2013).
[26] K. Jiménez-García, L. J. LeBlanc, R. A. Williams, M. C. Beeler, C. Qu, M. Gong, C. Zhang, and I. B. Spielman, Phys. Rev. Lett. **114**, 125301 (2015).
[27] X. Luo, L. Wu, J. Chenl, Q. Guan, K. Gao, Z. F. Xu, L. You, and R. Wang, Sci. Rep. **6**, 18983 (2016).
[28] Y. V. Kartashov, V. V. Konotop, M. Modugno, and E. Y. Sherman, Phys. Rev. Lett. **122**, 064101 (2019).
[29] Y. V. Kartashov and V. V. Konotop, Phys. Rev. Lett. **118**, 190401 (2017).
[30] M. C. Rechtsman, J. M. Zeuner, Y. Plotnik, Y. Lumer, D. Podolsky, F. Dreisow, S. Nolte, M. Segev, and A. Szameit, Nature (London) **496**, 196 (2013).
[31] Y. V. Kartashov, G. E. Astrakharchik, B. A. Malomed, and L. Torner, Nature Rev. Phys. **1**, 185 (2019).
[32] B. A. Malomed and D. Mihalache, Rom. J. Phys. **64**, 106 (2019).
[33] S. Blatt, T. L. Nicholson, B. J. Bloom, J. R. Williams, J. W. Thomsen, P. S. Julienne, and J. Ye, Phys. Rev. Lett. **107**, 073202 (2011).
[34] S. Inouye, M. R. Andrews, J. Stenger, H.-J. Miesner, D. M. Stamper-Kurn, and W. Ketterle, Nature (London) **392**, 151 (1998).
[35] S. V. Samsonov, A. D. R. Phelps, V. L. Bratman, G. Burt, G. G. Denisov, A. W. Cross, K. Ronald, W. He, and H. Yin, Phys. Rev. Lett. **92**, 118301 (2004).
[36] G. Burt, S. V. Samsonov, K. Ronald, G. G. Denisov, A. R. Young, V. L. Bratman, A. D. R. Phelps, A. W. Cross, I. V. Konoplev, W. He, J. Thomson, and C. G. Whyte, Phys. Rev. E **70**, 046402 (2004).